Cytotherapy, 2019; 21: 1033–1048

International Society
ISCT
Cell & Gene Therapy

FULL-LENGTH ARTICLES

Aggregation of human mesenchymal stem cells enhances survival and efficacy in stroke treatment

XUEGANG YUAN[1], JENS T. ROSENBERG[1,2], YIJUN LIU[1], SAMUEL C. GRANT[1,2] & TENG MA[1]

[1]*Department of Chemical and Biomedical Engineering; Florida State University, Tallahassee, Florida, USA, and*
[2]*The National High Magnetic Field Laboratory; Florida State University, Tallahassee, Florida, USA*

Abstract

Human mesenchymal stem cells (hMSCs) have been shown to enhance stroke lesion recovery by mediating inflammation and tissue repair through secretion of trophic factors. However, low cell survival and reduced primitive stem cell function of culture-expanded hMSCs are the major challenges limiting hMSC therapeutic efficacy in stroke treatment. In this study, we report the effects of short-term preconditioning of hMSCs via three-dimensional (3D) aggregation on stroke lesion recovery after intra-arterial (IA) transplantation of 3D aggregate-derived hMSCs (Agg-D hMSCs) in a transient middle cerebral artery occlusion (MCAO) stroke model. Compared with two-dimensional (2D) monolayer culture, Agg-D hMSCs exhibited increased resistance to ischemic stress, secretory function and therapeutic outcome. Short-term preconditioning via 3D aggregation reconfigured hMSC energy metabolism and altered redox cycle, which activated the *PI3K/AKT* pathway and enhanced resistance to *in vitro* oxidative stress. Analysis of transplanted hMSCs in MCAO rats using ultra-high-field magnetic resonance imaging at 21.1 T showed increased hMSC persistence and stroke lesion reduction by sodium (^{23}Na) imaging in the Agg-D hMSC group compared with 2D hMSC control. Behavioral analyses further revealed functional improvement in MCAO animal treated with Agg-D hMSCs compared with saline control. Together, the results demonstrated the improved outcome for Agg-D hMSCs in the MCAO model and suggest short-term 3D aggregation as an effective preconditioning strategy for hMSC functional enhancement in stroke treatment.

Key Words: *human mesenchymal stem cells, 3D aggregation culture, metabolic reconfiguration, PI3K/AKT pathway, ischemic stroke*

Significance

In this study, we report that short-term aggregation preconditioning enhanced hMSC resistance to ischemic stress and improved recovery in rat middle cerebral artery occlusion (MCAO) model. The findings reveal a novel mechanism of aggregation-mediated reconfiguration of metabolism and redox cycle in hMSCs, which led to the enhancement of stem cell properties. Aggregation-derived hMSCs exhibited enhanced therapeutic potential in MCAO model. This study demonstrates a potential preconditioning method to improve hMSC therapeutic efficacy in ischemic stroke treatment.

Introduction

Stroke is the fifth leading cause of death and primary cause of severe disability in the United States, with more than 795,000 individuals experiencing a new or recurrent ischemic episode each year [1,2]. Human mesenchymal stem cells (hMSCs) have attracted significant interest in stroke treatment and are considered the leading transplantable and clinically relevant cell type for stroke treatment because of their adult origin, availability, proven safety profile in clinical studies and neuroprotective and regenerative effects in the area of infarct [3]. However, significant challenges remain in supplying hMSCs of required

Correspondence: **Samuel C. Grant**, PhD, Department of Chemical & Biomedical Engineering, FAMU-FSU College of Engineering, 2525 Pottsdamer Street, Tallahassee, FL 32310. E-mail: grant@magnet.fsu.edu

(Received 13 December 2018; accepted 15 April 2019)

ISSN 1465-3249
https://doi.org/10.1016/j.jcyt.2019.04.055

therapeutic potency in stroke treatment. Recent studies reveal that the dosage used in hMSC clinical transplantation is significant lower than the threshold value needed [3], which is compounded by significant cell death post-transplantation in the stroke lesion. Studies have shown that only a small portion of transplanted stem cells (10–15%) survive 1 week post-transplantation and less than 3% survive after 28 days [4–8], significantly reducing the therapeutic efficacy. The mechanism of poor cell survival is multifactorial but is primarily attributed to the hostile ischemic tissue microenvironment characterized by proteases, inflammatory cytokines and elevated oxidative stress [9]. Thus, enhancing hMSC resistance to ischemic stress, while maintaining other cellular attributes such as secretory and migratory functions, is critical to improve their therapeutic efficacy.

Two-dimensional (2D) monolayer culture of hMSCs (hMSCs) is currently used to obtain sufficient cell number for therapeutic applications but is known to induce phenotypic changes with reduced therapeutic potential [10]. Preconditioning of hMSCs before transplantation has been pursued as a nongenetic means to enhance stem cell therapeutic effects [11]. Preconditioning of hMSCs with growth factors or pharmacological drugs has shown to increase *in vivo* persistence, secretory functions and functional recovery in ischemic stroke or cardiac injuries [12–17]. Additionally, hypoxic preconditioning of MSCs by short-term exposure to sub-lethal hypoxia (0.5% O_2) may improve therapeutic outcomes of stroke animals by enhancing the expression of trophic factors and increased cell viability under ischemic stress [18]. Compared with genetic manipulation, the nongenetic preconditioning strategies enhance hMSC properties without additional regulatory hurdles associated with genetic manipulation, but the extent of functional enhancement has been limited [11,19].

Recent discoveries suggest that three-dimensional (3D) hMSC aggregates, which are spheroids of tightly packed clusters of 500–10 000 cells, have reduced cell size, elevated secretion of anti-inflammatory and pro-regenerative cytokines, high resistance to ischemic stress, and increased *in vivo* migration [20]. Studies have demonstrated that both aggregates and aggregate-derived hMSCs (Agg-D hMSCs) were more effective than hMSCs from adherent cultures in modulating inflammatory reactions and improved recovery of myocardial infarction in mice [21]. Additionally, Agg-D hMSCs are smaller in size due to compaction [22], yielding about one-half the size of the adherent cells and thereby facilitating *in vivo* application. Aggregated hMSCs directly injected in rat myocardial infraction (MI) exhibited higher vascular endothelial growth factor (VEGF) expression and angiogenesis with reduced infract size [23]. Guo *et al.* further demonstrated that injection of Agg-D hMSCs attenuated brain stroke injury with reduced microinfarction compared with hMSCs from planar culture and attributed the beneficial effects to aggregation-mediated cell size reduction and increased neural differentiation [22,24]. Although these studies demonstrated the potential of Agg-D hMSCs in ischemic diseases, transplanted cell fate and impact on therapeutic efficacy remains unclear.

Magnetic resonance imaging (MRI) has excellent soft tissue contrast and is commonly used for stroke evaluation and diagnosis both in the clinic and preclinical research. The increased sensitivity afforded by high-field MRI provides not only higher spatial resolutions and shortened scan times but also allows for noninvasive tracking and monitoring of hMSC distribution and engraftment simultaneous to the evaluation of functional recovery at the ischemic lesion through ^{1}H and ^{23}Na imaging. Considering the importance of sodium in stroke pathology and the better than linear sensitivity increases expected with the quadripolar ^{23}Na nuclei [25,26], the use of high-field MRI, conducted here at 21.1 T, has the potential to identify ischemic regions beyond the acute stroke phase but before morphological changes are evident with ^{1}H MRI [27,28].

In this study, we tested the hypothesis that hMSC preconditioning by short-term aggregation (48 h) enhances efficacy in a rodent model of transient ischemia owing to the enhancement of cell survival and resistance to ischemic stress, migration and secretion of trophic factors. The results revealed that aggregation-induced changes in mitochondrial properties and redox balance with subsequent activation of *PI3K/AKT* play a central role in aggregation-mediated hMSC functional enhancement. MRI data show significant lesion recovery using ^{23}Na acquisitions while the traditional ^{1}H acquisitions had similar trends. Additionally, as the Agg-D hMSCs were labeled with micron-sized particles of iron oxides before injection, it was possible to evaluate their permanence in the ipsilateral hemisphere. Finally, behavioral characterization of motor function demonstrated functional recovery with Agg-D hMSC implantation. The results highlight the potential of 3D aggregation as a preconditioning strategy to enhance the efficacy of hMSC-mediated stroke lesion recovery.

Methods

hMSCs culture and 3D aggregation preconditioning

Standard frozen bone marrow–derived hMSCs at passage 3 in liquid nitrogen were obtained from the Tulane University Center for Stem Cell Research and Regenerative Medicine. hMSCs were isolated from the bone marrow of healthy donors ranging in age from 19 to 49 years based on plastic adherence, being negative for CD34, CD45, CD117 (all less than 2%) and positive for CD29, CD44, CD49c, CD90, CD105 and CD147

markers (all >95%) and possessing tri-lineage differentiation upon induction *in vitro* [22,29]. hMSCs were expanded with complete culture medium (CCM) composited with minimum essential medium-alpha (α-MEM) (Life Technologies, Carlsbad, CA) supplemented with 1% penicillin/streptomycin (Life Technologies) and 10% fetal bovine serum (FBS) (Atlanta Biologicals, Lawrenceville, GA) on 150-mm tissue culture petri dishes (Corning, Corning, NY) at a density of approximately 1500 cells/cm^2 in a standard 5% CO_2 incubator. The culture media were changed every 3 days. Cells were grown to 70−80% confluence and then harvested by incubation with 0.25% trypsin/EDTA (Invitrogen, Carlsbad, CA). Harvested cells were re-plated and subcultured up to passage 6. hMSCs at passages 5−6 were used in all experiments. To form 3D hMSC aggregates, hMSCs from adherent culture were harvested and re-suspended in CCM, and a total of 200 000 hMSCs were added into each well of an ultra-low attachment (ULA) six-well culture plates (Corning, Corning, NY) to form aggregates spontaneously. hMSC aggregates were incubated in a standard CO_2 incubator (37°C and 5% CO_2) for 48 h and then dissociated with 0.25% trypsin/EDTA (Invitrogen) to acquire single cell suspensions. Dissociated hMSCs from aggregates were cultured on tissue culture surface for recovery of 48 h under 37°C and 5% CO_2, and recovered hMSCs were defined as Agg-D hMSCs. On the basis of previous studies [20,22,30], the 48-h recovery following 3D aggregation culture was used to capture the functional enhancement of Agg-D hMSCs, provide comparable uniformity between the Agg-D and 2D hMSCs, and generate a sufficient and comparable cell number for *in vivo* study. All reagents were purchased from Sigma Aldrich (St. Louis, MO) unless otherwise noted.

NADH and NADPH measurement, CFU-F assay, mitochondrial membrane potential and complex I activity

Nicotinamide adenine dinucleotide (NAD+) and its reduced form NADH was measured by an NAD/NADH Quantitation Colorimetric Kit (BioVision, Milpitas, CA) following the vender's protocol. Briefly, hMSCs were pelleted and lysed by NADH extraction buffer by two cycles of freeze/thaw. To detect NADH, NAD was decomposed at 60°C water bath for 30 min. The extracted samples were transferred in a 96-well plate and NAD cycling enzyme mix and NADH developer were added to the standard and sample for reaction to occur at room temperature for 4 h of development. The plate was read at an optical density (OD) of 450 nm using the iMarkTM microplate reader (BioRad, Hercules, CA). The reading was normalized to the standard curve and cell number. Nicotinamide adenine dinucleotide phosphate (NADP+) and its reduced form NADPH were measured via an NADP/NADPH Quantitation Kit (Sigma Aldrich, St. Louis, MO) following the procedure provided by the assay kit. Mitochondrial complex I activity was determined using the Complex I Enzyme Activity Microplate Assay Kit (Abcam, Cambridge, MA). Colony-forming unit fibroblast (CFU-F) numbers and mitochondrial membrane potential and were determined by following the method reported previously [30].

Intracellular adenosine triphosphate content measurement and transwell migration assay

hMSCs were harvested and re-suspended in DI water, and heated immediately in a boiling water bath for 15 min. The mixture was centrifuged, and the supernatant was collected. Upon measurement, 10 mL of sample solution was mixed with 100 mL of the luciferin-luciferase reagent, and the bioluminescent signal was measured using an Orion Microplate Luminometer (Bad Wildbad, Deutschland, Titertek Berthold, Pforzheim, Germany) after 15 min incubation at room temperature. For inhibition of glycolysis, 2-deoxyglucose (2-DG, Sigma Aldrich, St. Louis, MO) was used to treat cells at 5 mmol/L for 24 h. A transwell migration system (Neuro Probe, Gaithersburg, MD) was used to study the migration of Agg-D hMSCs and 2D hMSCs in response to human recombinant stromal cell-derived factor 1 (R&D Systems, Minneapolis, MN) following manufacture instructions.

Survival test under ischemic condition in vitro *and* PI3K/AKT *inhibitor treatment*

Cell survival was determined by a Live/Dead staining kit (Thermo Fisher Scientific, Waltham, MA). hMSCs were stained with 1 μmol/L calcein AM (green) and 2 μmol/L ethidium homodimer I (red) and incubated at 37°C for 15 min to differentiate live (green) and dead cells (red) using a fluorescent microscope (Olympus, Center Vally, PA). For the inhibition of *PI3K* and *PTEN*, LY294002 (20 μmol/L) and SF1670 (10 μmol/L) were used, respectively, to treat hMSCs for 24 h. Treated hMSCs were exposed to *in vitro* ischemia or H_2O_2 condition for an additional 6 or 24 h. For *in vitro* ischemic treatment, cells were cultured under 1% O_2, 5% CO_2 and balanced N_2 in a C-Chamber (BioSpherix, Lacona, NY) with serum-deprivation culture medium. For H_2O_2 treatment, cells were cultured with 200 μmol/L H_2O_2 in CCM [23,29].

Real-time reverse transcriptase-polymerase chain reaction

Gene expression was carried out following protocols outlined in our previous studies [22,29]. Briefly, total RNA was isolated using the RNeasy Plus kit (Qiagen,

Valencia, CA) following the manufacturer's instructions. Reverse transcription was carried out using 2 μg of total RNA, anchored oligo-dT primers (Operon, Huntsville, AL) and Superscript III (Life Technologies). Primers specific for target genes were designed using the software Oligo Explorer 1.2 (Genelink, Hawthorne, NY), and Beta-actin was used as an endogenous control for normalization. Real-time reverse transcriptase-polymerase chain reaction (RT-PCR) reactions were performed on an ABI7500 instrument (Applied Biosystems, Foster City, CA), using SYBR Green PCR Master Mix. The amplification reactions were performed, and the quality and primer specificity were verified. Fold variation in gene expressions were quantified using the comparative Ct method: $2^{-(\mathrm{CtTreatment}-\mathrm{CtControl})}$, which is based on the comparison of the expression of the target gene (normalized to beta-actin).

Rat middle cerebral artery occlusion model

Middle cerebral artery occlusion (MCAO) was performed following the procedures by Longa *et al.* and Uluç *et al.* [31,32]. All surgical procedures were carried out under aseptic conditions and approved by the Florida State University Animal Care and Use Committee. Briefly, juvenile male Sprague-Dawley rats weighing between 200 and 250 g were anesthetized with 5% isoflurane in an actively scavenged induction chamber and maintained on 2–3% isoflurane during the surgical procedure. The common carotid artery, external carotid artery (ECA) and internal carotid artery (ICA) were exposed by blunt and sharp dissection. A 3.0-cm filament with a 0.39-mm-thick and 2- to 3-mm-long rubber coating (Doccol Corp, Redlands, CA) was inserted through the ECA. The filament was guided 1.9 cm into the ICA until the MCA was blocked. The transient occlusion occurred for 1 h, followed by removal of the filament.

hMSC labeling and transplantation

hMSCs were washed with phosphate-buffered saline (PBS) and then 20 mL of fresh CCM with 167 μL (corresponding to 7.47 μg Fe/mL) of micron-sized particles of iron oxides (MPIO; Bangs Laboratories, Fishers, IN) used to label the cells for MRI tracking. The MPIO are tagged with a red fluorescence marker (660/690 nm; diameter: 0.86 μm) [33,34]. For Agg-D hMSCs, a 12-h incubation with MPIO was conducted during the last phase of the 48-h recovery after dissociation and replating on tissue culture surfaces. After incubation, hMSCs were washed with sterile PBS thoroughly to eliminate the extracellular MPIO particles and harvested using with 0.25% trypsin/EDTA, and then 1×10^6 labeled cells were re-suspended in 50 μL sterile PBS for transplantation.

IA injections were performed immediately after the MCAO using the exposed ECA. Before injection, the pterygopalatine artery (PPA) was clamped with a microvascular clamp. Injections were performed with a 33-G custom-made needle and 50-μL syringe (Hamilton Company, Reno, NV) loaded with 1×10^6 MPIO-labeled hMSCs resuspended in 50 μL sterile PBS. Over a 1-min period, cells were injected in the ICA just rostral to the ECA–ICA bifurcation. A gel-foam (Pharmacia & Upjohn, Kalamazoo, MI) was used during needle extraction to prevent bleeding. The incision was sutured following administration of analgesia (Bupivacaine, Hospira Inc., Lake Forest, IL), and rehydration was used to minimize pain and discomfort post-surgery. To serve as an untreated control, 50-μL PBS was injected instead of cells as an MCAO-PBS group (n = 5) for comparison to the Agg-D hMSC groups (n = 7) and a 2D hMSC group (n = 7) prepared without aggregation. The immediate injection of hMSCs or PBS following the filament removal was performed to minimize pain and discomfort as well as the number of surgical procedures and total time under anesthesia for the animals. This approach precluded pretesting of the severity of the MCAO-induced ischemia before their inclusion in specific experimental groups, which was defined by the type of injection received. The presence of ischemic injury, however, was confirmed by 24-h MRI and behavioral tests after MCAO and IA injection.

In vivo *MR Imaging*

Images were acquired using an ultra-wide-bore 21.1-T, 900-MHz vertical magnet equipped with a Bruker Avance III console and Paravision 5.1 (Bruker-Biospin, Billerica, MA) [35]. All animals were imaged with a custom-built, double tuned 33-mm radio frequency (RF) coil resonating at 900 MHz for ^{1}H and 237 MHz for ^{23}Na. The RF coil was attached to a custom-built probe body and bite-bar to which the animal was suspended while supplying continuous flow of oxygen and anesthesia (isoflurane). The probe was equipped for respiration monitoring (SA Instrument, Stonybrook, NY) and triggering enabled to minimize motion artifacts. Imaging was performed to evaluate stroke lesion size with ^{1}H and ^{23}Na sequences and to visualize MPIO-labeled hMSCs with 2D T_2-weighted spin echo (SE), 3D gradient recalled echo (GRE) and a diffusion-weighted 2D SE for apparent diffusion coefficient (ADC) measurements. For ^{1}H stroke lesion imaging, a 2D T_2-weighted spin echo (SE) sequence was used with fat suppression and respiratory gating to minimize motion

artifacts. Acquisition parameters were echo time/repetition time (TE/TR) = 26/6000 ms, 25 slices with a thickness of 0.5 mm in anatomic axial orientation with 100 × 100−μm in-plane resolution. ^{23}Na imaging was performed with a 3D GRE sequence with TE/TR = 1/50 ms, 1-mm isotropic resolution and 36 averages, resulting in a 35-min scan. For imaging of MPIO-labeled cells, a 2D GRE sequence was used with TE/TR = 5/750 ms, 35 slices with a thickness of 0.3 mm in axial orientation and 50 × 50-μm in-plane resolution. For ADC measurements on the Agg-D hMSC and MCAO-PBS groups, diffusion-weighted 2D echo planar images (EPI) were acquired in the anatomical coronal direction with TE/TR = 45.3/6000 ms and 320 × 320−μm in-plane resolution with 1.0-mm slice thickness. Diffusion gradient duration (δ) was 3.5 ms, and the diffusion gradient separation was (Δ) was 9.8 ms. Four b values of 0, 200, 600 and 1000 s/mm^2 were used to calculate ADC on one central slice over the stroke. The same slice and slice position were processed for all animals and time points. The total scan time was about 2 h. Control (MCAO-PBS) and Agg-D hMSCs groups were imaged 24 h, 72 h and 1 week post-surgery, whereas 2D hMSCs groups were imaged 24 h and 1 week post−ischemic injury.

Ex Vivo *MR Imaging*

After the last imaging session, the animal was sacrificed and trans-cardinally perfused with 4% paraformaldehyde. After a 48-h immersion in paraformaldehyde, the decapitated head was washed with PBS, immersed with in a non-protonated fluorocarbon (FC-43, 3M Corp, Minneapolis, MN) and imaged at 11.75 T using a 3D GRE sequence at 100-μm isotropic resolution (TE/TR = 7.5 and 150 ms). The intent of the 3D GRE scan is to provide verification of the presence of MPIO-labeled cells at the 1-week time point.

Imaging processing

Animals with an initial stroke lesion between 10 and 65 mm^3 were chosen to be included in the study leaving a total of five MCAO-PBS animals and seven animals injected with MPIO-labeled Agg-D or 2D hMSCs. The stroke lesion size was analyzed by manually tracing the edge of the hyperintense lesion in T_2-weighted ^{1}H and ^{23}Na images using Amira 5.3.4 (Visualization Sciences Group, Burlington, MA) and presented as the average percent decrease in lesion volume. The presence of MPIO-labeled cells was quantified based on the signal voids created by the MPIO in T_2*W GRE images. Using AMIRA, a non-local means filter was applied in plane to reduce noise. Pixels were defined as being part of a MPIO-labeled cell if any of its signal were less than the average signal of a region of interest (ROI) on the contralateral side minus three times its standard deviation as described in Equation 1.

$$\textit{MPIO labeled cells} \equiv \overline{S}_{Contrlateral} - 3 * \sigma_{ContraLateral} \qquad (1)$$

Any obvious noise region detected was excluded in the volumetric measurements by manual assessment. To adjust for pixels mistaken for MPIO-labeled cells such as arteries, the volume from each animal was subtracted from the average volumes of the control group. Data are presented as the average percent volume decrease over the two imaging sessions. Using Paravision 5.1, diffusion-weighted images were analyzed by placing a ROI around the lesion on the central slice as visualized by a weighted image. The same slice and slice position were used for all time points for accurate comparison of the lesion regression. Data are presented as the average percent decrease between the time points.

Behavioral tests

To further assess the functional recovery of post-transplanted MCAO rats, open field test (OFT), elevated plus maze (EPM) and cylinder test were performed for each animal at the following time points: before surgery (0 week), 1, 2, 3 and 4 weeks after MCAO and cell transplantation. Behavioral assessments were performed on three groups: a sham group that received all procedures except the placement of the filament to achieve MCAO and cell injection (n = 6), an Agg-D hMSC group (n = 4), and a MCAO-PBS group (n = 5). The animals used in behavioral measurements represent a cohort separate from those that underwent full MR evaluations, hence the differences in group numbers. At the beginning of behavioral testing, each group contained six animals. Animals were scanned once with MRI at 48 h post-MCAO to verify the presence of an ischemic lesion and successful injection of hMSCs (if applicable). If appropriate MR requirements were not met, animals were eliminated from the behavioral study. Also, during the progression of behavioral characterization, certain specimens were eliminated from the behavioral study as a result of either non-compliance (one for Agg-D hMSCs and one for MCAO-PBS) or if pre-determined endpoints for euthanasia during the 4-week behavioral period necessitated sacrifice (one for Agg-D hMSCs).

Animals were placed in the experimental environment for 1 h before behavioral tests. All experiments were carried out under white light during the time between 9:00 am to 5:00 pm. For OFT, a 90 × 90-cm square arena divided into 36 spaces was used (defined as outer, middle and center zone). At the beginning of the test, the animal was placed in the center zone and

all movements were recorded by video-tracking camera during a 5-min session. The EPM consisted of a central area (8.5 cm × 8.5 cm) connected to two open arms (50 cm × 8.5 cm) and two closed arms (50 cm × 8.5 cm) placed in a plus-shape structure and elevated 50 cm above the floor. Animals were placed in the central area of the maze, and all movements were recorded by video-tracking camera during a 5-min session. Forelimb locomotor test was performed using a transparent cylinder of 50-cm height and 15-cm diameter. At the beginning of the test, the animal was placed at the bottom of the cylinder and all the movements was recorded by a video-tracking camera. Three categories of movement were recorded: independent ipsilateral forelimb use (I), independent contralateral forelimb use (C) and both forelimbs in use (B). The test was quantified using the Limb Use Asymmetry Score calculated by the following equation:

$$Score = \frac{I}{I+C+B} - \frac{C}{I+C+B} \quad (2)$$

Statistics/data analysis

Unless otherwise noted, all experiments were performed at least in triplicate (n = 3), and representative data are presented. Experimental results are expressed as means ± SD of the samples. Statistical comparisons were performed by one-way analysis of variance and Tukey's post hoc test for comparisons, and significance was accepted with $P < 0.05$.

Results

hMSCs aggregation enhances a spectrum of cellular properties

Agg-D hMSCs were recovered for 48 h before being tested for *in vitro* experiments. Compared with 2D planar culture, Agg-D hMSCs are significantly smaller in size (Figure 1A, B) with a spindle shape. Agg-D hMSCs also showed reduced senescence and enhanced CFU-F ability compared with 2D hMSCs, as shown in Figure 1C and 1D. Enhanced migratory ability via transwell assay along with up-regulated C-X-C chemokine receptor type 4 (CXCR4) expression also were observed in Agg-D hMSCs (Figure 1E, F). Hepatocyte growth factor (HGF) and VEGF genes were up-regulated after 3D aggregation culture (Figure 1G, H), along with other functional cytokine secretions reported in our prior work [30,36,37].

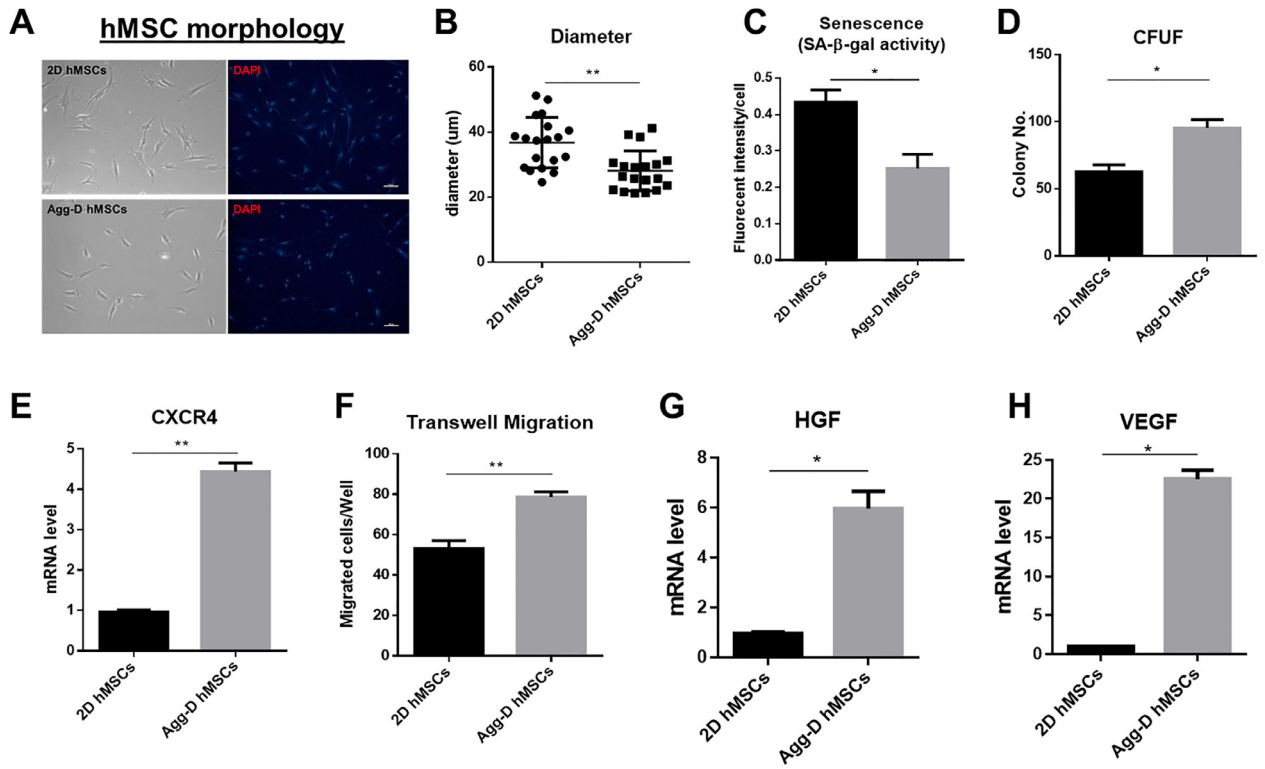

Figure 1. hMSC preconditioning via 3D aggregation restores primitive hMSC properties. (A) Representative images of 2D hMSCs and reseeding of Agg-D hMSCs on 2D culture plates. Scale bar is 100 μm. (B) Cell size of 2D versus Agg-D hMSCs. (C) Senescence of 2D versus Agg-D hMSCs after re-seeding on 2D culture plates based on beta-gal activity. (D) CFU-F number of 2D and Agg-D hMSCs after 12 days of culture. (E) Expression of CXCR4 gene in 2D versus Agg-D hMSCs. (F) Transwell migration of 2D versus Agg-D hMSCs. (G) and (H) Expression of HGF and VEGF genes in 2D versus Agg-D hMSCs. *$P < 0.05$; **$P < 0.01$.

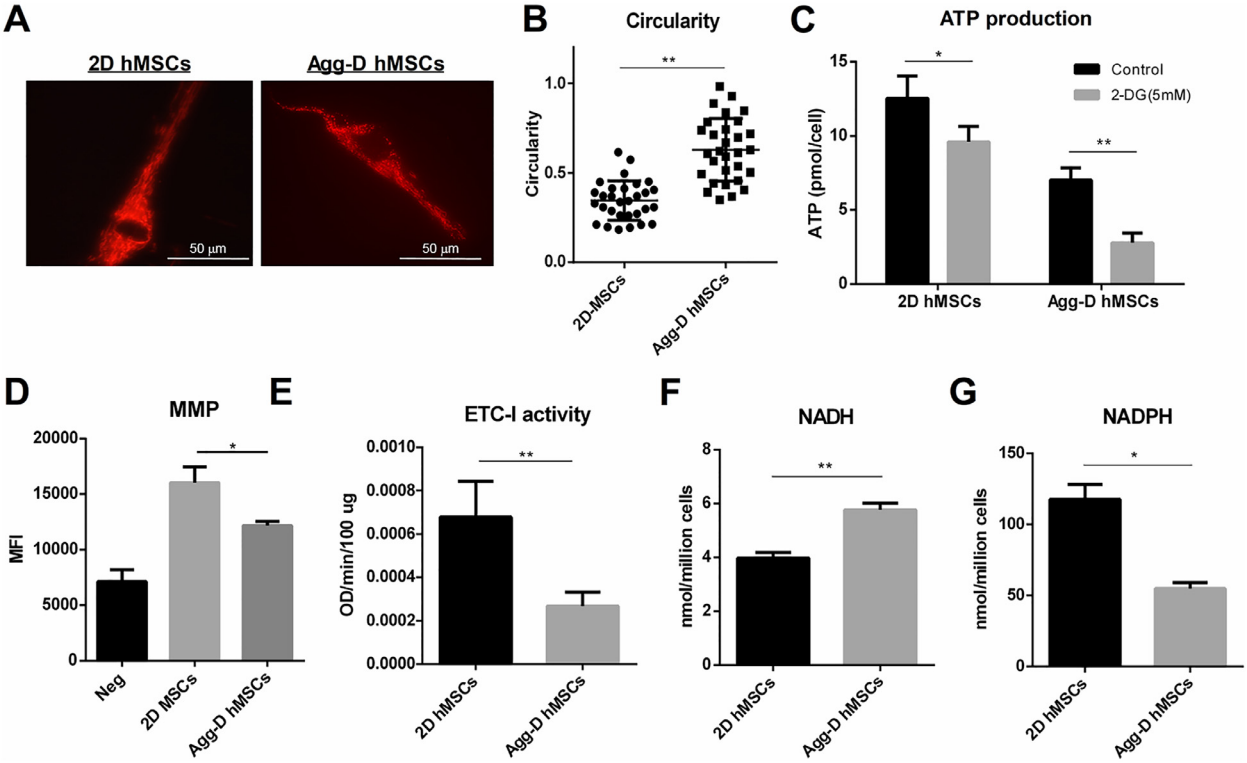

Figure 2. Mitochondrial function and redox cycle alteration in 2D and Agg-D hMSCs. (A) Representative images of mitochondrial morphology in 2D versus Agg-D hMSCs, stained with Mitotracker Red, taken at × 100. Scale bar is 50 μm. (B) Circularity of mitochondria in 2D versus Agg-D hMSCs. (C) ATP content with or without 2DG treatment in 2D versus Agg-D hMSCs. (D) Mitochondrial membrane potential measured by flow cytometry. (E) Electron transport complex I activity. (F) NADH and (G) NADPH levels in 2D versus Agg-D hMSCs. $*P < 0.05$; $**P < 0.01$.

hMSCs aggregation changes mitochondrial properties and redox balance

Agg-D hMSCs exhibited fragmented mitochondrial morphology compared with 2D controls, as shown in Figure 2A and 2B. Agg-D hMSCs also have lower total adenosine triphosphate (ATP) content while the percentage of glycolytic ATP is higher compared with 2D hMSCs (Figure 2C), suggesting increased glycolysis in Agg-D hMSCs. Analysis of mitochondrial membrane potential and electron transport complex I activity (Figure 2D, E) revealed reduced mitochondrial function in Agg-D hMSCs compared 2D control, which is further corroborated by increased NADH and reduced NADPH level (Figure 2F, G). These results demonstrated that Agg-D hMSCs have reduced mitochondrial activity and altered redox status compared with 2D planar cultured hMSCs.

Agg-D hMSCs have increased expression of survival and anti-apoptotic genes, and enhanced resistance to ischemia and reactive oxygen species–enriched environment

Aggregation preconditioning induced robust up-regulation of *PI3K* and *AKT* genes with a corresponding reduction in *PTEN* expression compared to 2D controls (Figure 3A). As a result of *PI3K/AKT* activation, several pro-survival and anti-apoptotic genes such as *BCL-2*, *BCL-XL*, *ERK1/2*, *HIF-1α* and *NF-κB* also were up-regulated in Agg-D hMSCs, whereas pro-apoptotic gene such as *P53* and *BAX* were down-regulated (Figure 3B, C). To test the survival of Agg-D hMSCs under ischemia or high reactive oxygen species conditions *in vitro*, cells were cultured under standard ischemia in CCM without FBS or treated with hydrogen peroxide (H_2O_2), respectively, to determine the effects of oxidative stress on cell viability. Survival rate determined by Live/Dead staining showed that Agg-D hMSCs have higher cell survival rate with fewer cells with damaged plasma membranes (Figure 4A, C) under ischemia and ROS-enriched environments. These trends were confirmed by DNA assay with 52% and 50.8% more cell survival after culture under ischemia and H_2O_2 treatment for 6 h, respectively (30% and 71%, respectively, at 24 h), as shown in Figure 4B and 4D.

Aggregation-mediated activation of PI3K/AKT *pathway is required for hMSC survival and resistance to ischemic stress*

To further investigate *PI3K/AKT* signaling pathway in regulating survival of Agg-D hMSCs under ischemic

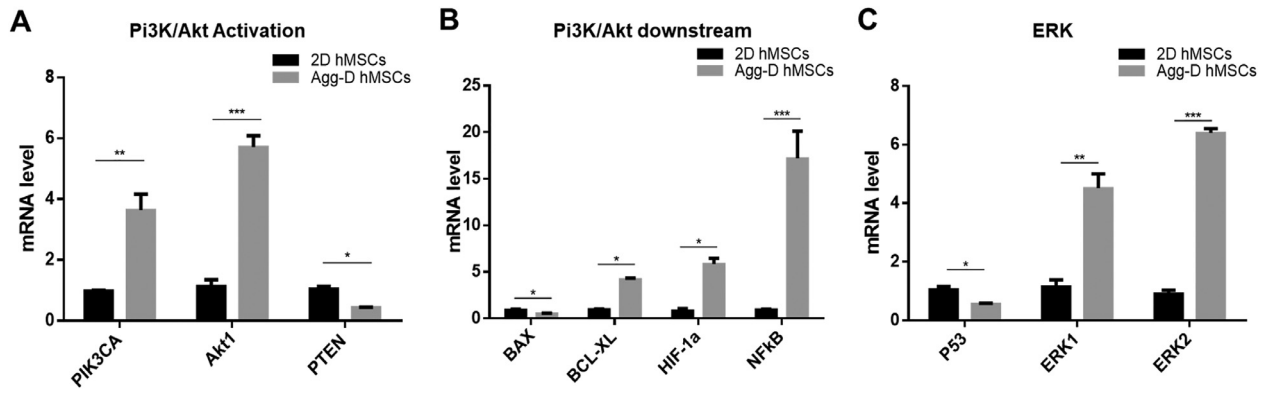

Figure 3. Aggregation-mediated activation of *PI3K/AKT* pathway and increased anti-apoptotic activity. (A) *PI3K*, *AKT* up-regulation and *PTEN* down-regulation in Agg-D compared with 2D hMSC. (B) Increased expression of anti-apoptotic genes downstream of *PI3K/AKT* pathway in Agg-D hMSC compared with 2D hMSCs. (C) Reduced expression of *P53* and increased *ERK1/2* in Agg-D compared with 2D control hMSCs. $*P < 0.05$; $**P < 0.01$; $P < 0.001$.

conditions, Agg-D hMSCs and 2D controls were treated with a small molecule *PI3K* inhibitor, LY294002, and *PTEN* inhibitor, SF1670. LY294002 inhibits *PIP2* to *PIP3* conversion in *PI3K* activation, whereas SF1670 had an opposite effect and reactivated *PI3K/AKT* pathway [38]. There is a clear decrease of survival rate of Agg-D hMSCs after ischemia and H_2O_2 treatment with *PI3K* inhibition (Figure 5A, B). With SF1670 treatment, both Agg-D and 2D control hMSCs exhibited higher survival rate under oxidative stress as *PI3K/AKT* was reactivated via inhibition of *PTEN* (Figure 5C, D).

Agg-D hMSCs have increased in vivo *persistence and reduced lesion size in MCAO stroke model*

To analyze the fate of transplanted Agg-D hMSCs and its effects on stroke lesion recovery, ^{1}H and ^{23}Na

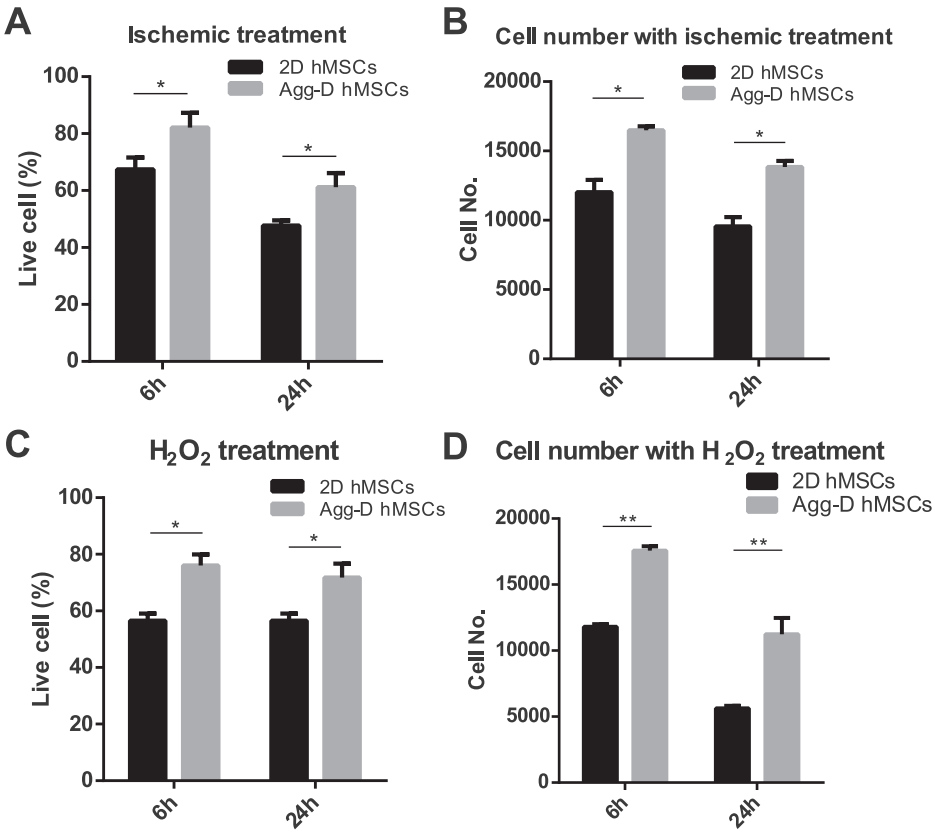

Figure 4. Three-dimensional aggregation culture enhances hMSC resistance to *in vitro* ischemic and ROS-enriched environment. (A) and (C) Cell survival under *in vitro* ischemia for 6 and 24 h based on Live/Dead staining and DNA assay, respectively. (B) and (D) Cell survival under H_2O_2 treatment for 6 and 24 h based on Live/Dead staining and DNA assay, respectively. $*P < 0.05$; $**P < 0.01$.

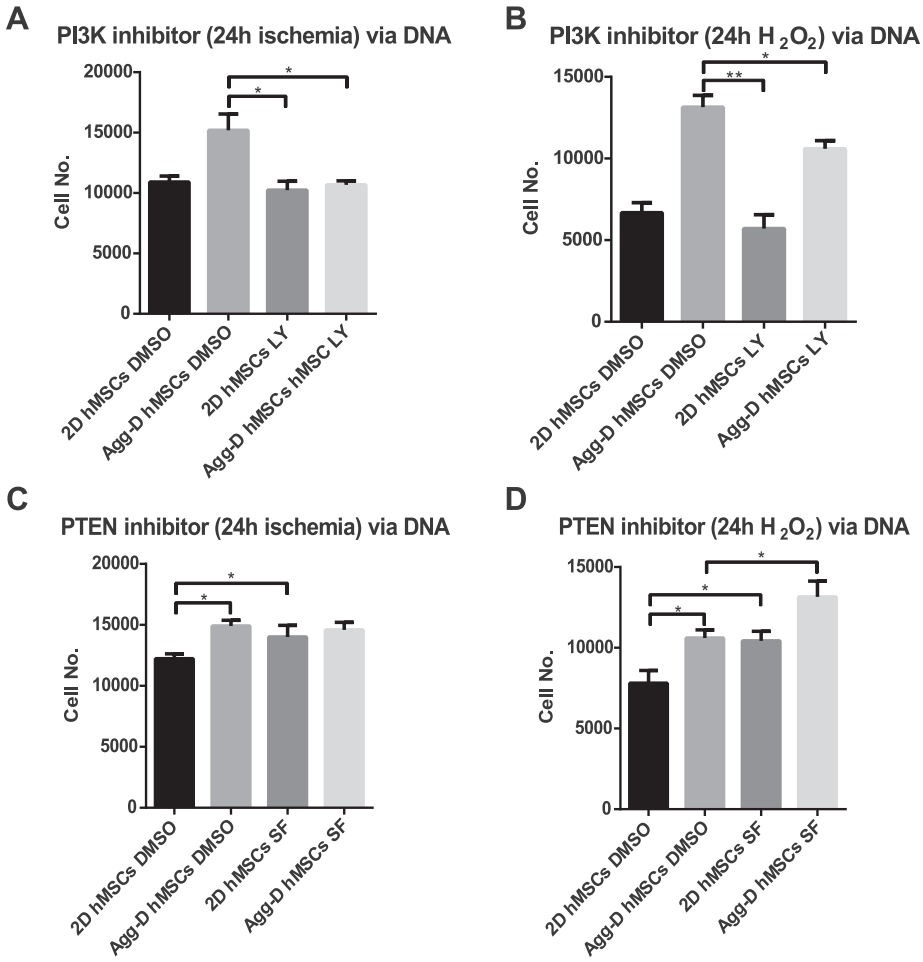

Figure 5. Activation of *PI3K/AKT* influences hMSC resistance to *in vitro* ischemia stress. (A) and (B) Inhibition of *PI3K/AKT* pathway via LY29004 attenuates Agg-D hMSC survival under 24 h *in vitro* ischemia or H_2O_2 treatment. (C) and (D) Inhibition of *PTEN* via SF1670 enhanced survival of Agg-D and 2D control hMSCs after 24 h *in vitro* ischemia or H_2O_2 treatment. $^{\star}P < 0.05$; $^{\star\star}P < 0.01$.

MRI were performed at days 1, 3 and 7 post-transplantation for Agg-D hMSCs and MCAO-PBS animals, as shown in Figure 6A. One week after transplantation, the lesion volume as determined by T_2-weighted proton MRI decreased 68.7% in the Agg-D hMSC group compared to 59.6% in the MCAO-PBS group, but the difference was not statistically significant (Figure 6B). In contrast, the lesion volume as determined by ^{23}Na imaging showed statistically significant decrease in the Agg-D hMSC group (81.4%) compared with 39.7% in MCAO-PBS group (Figure 6B), indicative of the re-establishment of sodium homeostasis and normal ionic gradients with Agg-D hMSC injection. To analyze the fate of transplanted hMSCs, *in vivo* $T_2^{\star}$-weighted GRE acquisitions were carried out and the fraction of signal voids created by the labeled hMSCs was used as a surrogate for the retention of implanted hMSCs relative to the 24-h time point. Although not statistically significant, as shown in Figure 6C, a 57% reduction in signal voids was observed in the Agg-D hMSC group compared to 65.8% in the 2D hMSC group. As expected, the stroke lesion, due to the restriction of intracellular water, displayed a lower ADC compared with the contralateral side. An increase in ADC also was observed for all groups after 1 week for all measurements on the ipsilateral side. However, the Agg-D hMSC group shows a significant recovery after 7 days, whereas MCAO-PBS group has minimal recovery with no significance. The noninvasive MRI results indicate a positive response for Agg-D hMSCs with respect to stroke lesion volume and improved functional metrics for by both ^{1}H and ^{23}Na acquisitions. To confirm the *in vivo* contrast of MPIO-labeled Agg-D hMSCs and retention of labeled cells after one week, high-resolution *ex vivo* 3D GRE scans were performed on all animals. Figure 6E shows a representative image from a MCAO animal that received Agg-D hMSCs. The resolution of this 3D image displays the retention of MPIO contrast, which reflects the presence of injected hMSCs, out to 1 week.

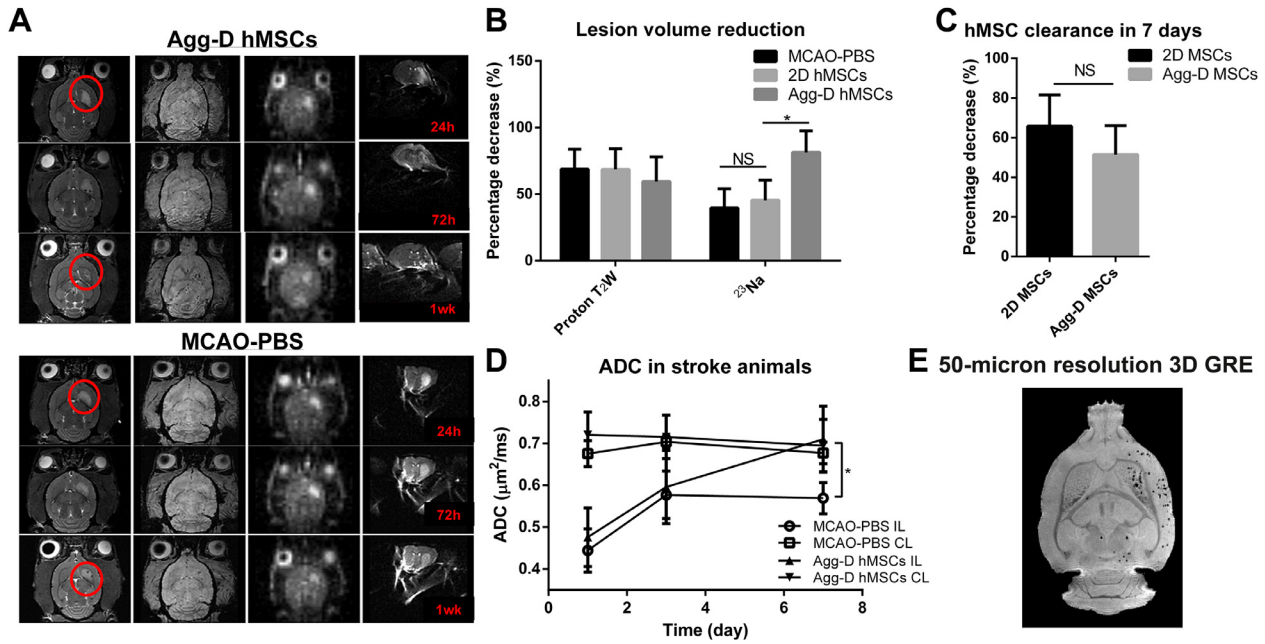

Figure 6. MRI demonstrated stroke lesion recovery and cell clearance after transplantation of Agg-D hMSCs in MCAO animals. (A) Representative *in vivo* MRI image of T_2-weighted, 2D GRE, 3D-^{23}Na and 2D diffusion weighted echo planner image (EPI) of Agg-D hMSCs and MCAO-PBS group at 1, 3 and 7 d after MCAO and injection. (B) Lesion volume reduction calculated from proton T_2 weight and ^{23}Na image. (C) Cell clearance of Agg-D and 2D hMSCs 7 days after transplantation. (D) Apparent diffusion coefficient (ADC) of Agg-D hMSCs and MCAO-PBS group. (E) *Ex vivo*, high-resolution (100-μm isotropic) 3D GRE images of a perfused MCAO rat that was injected with Agg-D hMSCs showing the retention of MPIO-labeled cells after 1 week. n = 7 for 2D and Agg-D hMSC group, n = 5 for MCAO-PBS group. NS, not significant; $^*P < 0.05$. CL, contralateral; IL, ipsilateral.

Agg-D hMSCs improved neurological functional recovery in MCAO rat

To evaluate the neurological function recovery of MCAO animal after transplantation of Agg-D hMSCs, behavioral assessments included open field, elevated plus maze and forelimb use asymmetry (cylinder) tests. For the OFT, both stroke-control group and Agg-D hMSC group showed significant declines of entry at early time points compared to the Sham group (Figure 7A). However, the Agg-D hMSC group exhibited recovered locomotion activity demonstrated by increased entries and exploration at 2 weeks after transplantation, although there was no significant difference compared with the MCAO-PBS group. At week 4, the Agg-D-hMSC group shows significantly improved locomotion activity with longer travel distance and less spontaneous exploration at the outer zone of the open field compared with MCAO-PBS group (Figure 7B, C). Similar results were observed in the EPM test for examination of explore-related behavior. The Agg-D hMSC group has increased entries of the open arm following transplantation, but a significant difference was observed starting at week 3 (Figure 7D). The Agg-D hMSC group also had longer travel distance and spent more time in open arms compared with the stroke control group (Figure 7E, F). Figure 7G demonstrated the representative behavioral pattern of different groups of animals at week 4. Asymmetry score was calculated based on the cylinder test for the impairment of forelimb use. As Figure 7H shows, animals receiving Agg-D hMSCs have lower asymmetry score compare with MCAO-PBS group; in fact, no obvious recovery for the MCAO-PBS group was observed over 4 weeks. These results demonstrate enhanced functional recovery of stroke animals after Agg-D hMSC transplantation.

Discussion

In response to injury cues, the transplanted hMSCs migrate to the injury site and mediate tissue regeneration primarily by the delivery of trophic and paracrine factors [39]. As a result, both *in vivo* persistence and secretory functions of transplanted hMSCs are critical to the therapeutic outcome. However, conventional *in vitro* hMSC expansion on 2D surface is known to alter these properties and reduce their therapeutic efficiency. For example, transplantation of culture-expanded hMSC has very low engraftment and homing efficiency, with <0.001% of total injected cells surviving and homing to the ischemic cortex in rats [40,41]. Culture expansion also induces cellular senescence with altered secretory profile and enlarged cell size, adversely influencing their efficacy in stroke

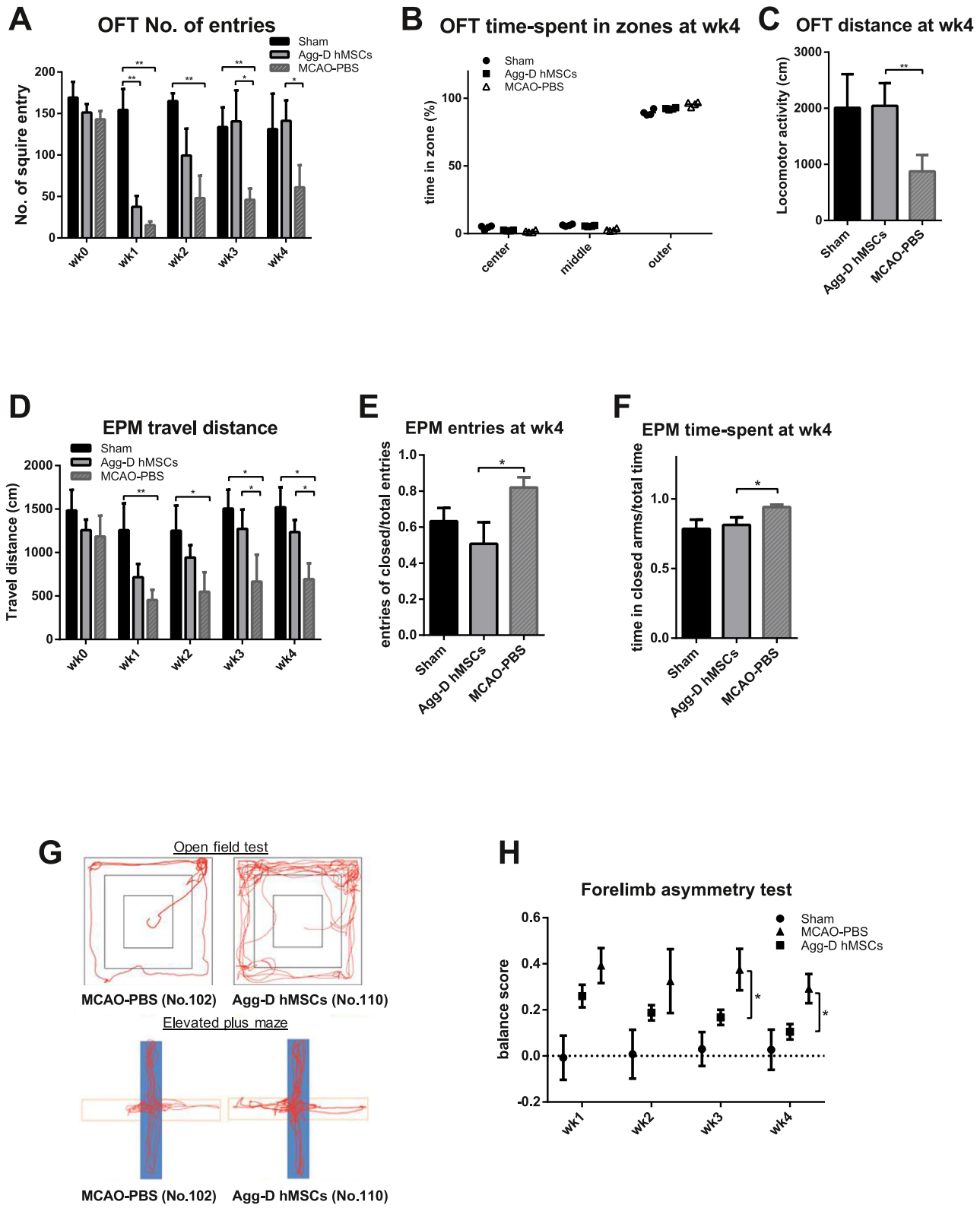

Figure 7. Functional recovery of MCAO animals after transplantation of Agg-D hMSCs. (A) Number of entries in open field test from week 0 to 4. (B) Time spent in different zones at week 4. (C) Travel distance in open field test at week 4. (D) Travel distance in elevated plus maze from week 0 to week 4. (E) Number of entries in open arm/total entries for elevated plus maze at week 4. (F) Time spent in closed arm/total time for elevated plus maze at week 4. (G) Representative trace of animals traveled in open field test and elevated plus maze for MCAO-PBS group and Agg-D hMSC group. (H) Asymmetrical score calculated from cylinder test from week 0 to 4. n = 6 for sham group, n = 4 for Agg-D hMSC group, and n = 5 for MCAO-PBS group. $*P < 0.05$; $**P < 0.01$.

treatment [42]. Therefore, maintaining migration and secretory properties of culture-expanded hMSCs have been important challenges in large-scale hMSC manufacturing for clinical application [43,44]. Compared with a genetic transfection strategy targeting pro-mitogenic and anti-apoptotic genes, nongenetic preconditioning such as exposure to sublethal oxygen tension or pharmacological agents potentiates hMSC therapeutic effectiveness without additional safety concerns or regulations [11,18]. The results of the current study show that a short duration of aggregation preconditioning (~48 h) enhances several critical cellular properties including cell size, migration, secretory functions and *in vivo* survival, which together enhance the efficacy of hMSC-based stroke treatment [20].

The size of transplanted hMSCs significantly influences therapeutic outcome because large cells introduced into the cerebral vascular system could lead to random embolisms or even lacunar stroke [45,46]. In the current study, the diameters of Agg-D hMSCs are approximately 45% of the 2D-cultured hMSC size after 2-day aggregation culture as previously reported [22,24] and maintain this reduced size after reseeding and 2-day expansion on planar culture. Prior studies have shown that actin-mediated compaction plays a central role in hMSC aggregation [30] and is responsible for reduced cell size of Agg-D hMSCs compared with 2D controls [30,36,47]. A recent study suggests that hMSC aggregation induced autophagy [48] and increased secretome in 3D aggregates, reducing hMSC size [49]. Thus, multiple mechanisms could be involved in regulating hMSC size after aggregation, and additional studies are warranted to understand the underpinning mechanism.

After 2 days of planar culture and before injection, Agg-D hMSCs still maintained higher CXCR-4 expression and migration with elevated VEGF and HGF secretion, suggesting the durable effects of aggregation on hMSC migration and secretory functions. Hypoxia preconditioning has been found to be effective in enhancing hMSC migration and secretory functions, but the specific level of oxygen tension and fluctuation in oxygen tension adversely affects hMSC properties [50]. Because maintaining a constant level of reduced oxygen tension is a challenge in clinical implementation, aggregation is a more potent and implementable strategy to enhance hMSC properties.

Aggregation-induced changes in mitochondrial properties and alteration in redox balance activate the *PI3K/AKT* pathway and subsequently up-regulate anti-apoptotic and cell survival genes such as *BCL-XL*, *ERK1* and *ERK2* (Figs. 3–5). *PI3K/AKT* is a key signaling pathway that regulates cell survival, apoptosis, migration and secretory functions [51], and has been targeted in various hMSC preconditioning strategies, such as hypoxia, growth factor treatment and aggregation [52-55]. *PI3K/AKT* is shown to be activated through *PTEN* inhibition because of mitochondrial respiration defects and NADPH/NADH redox imbalance [54]. Our results show that hMSC aggregation significantly reduces mitochondrial membrane potential and complex I (ETC-I) activity with altered cellular NADH and NADPH levels (Figure 2), which could activate the *PI3K/AKT* pathway, affording Agg-D hMSCs a survival advantage against ischemic stress. It is well established that energy metabolism regulates cellular homeostasis and functional properties. Our previous studies have shown that clonogenic hMSCs are characterized by high aerobic glycolysis activity and that aerobic glycolysis is required to sustain hMSC's anti-inflammatory properties [55]. Similarly, aggregation culture supports the reacquisition of primitive hMSC properties in 3D hMSC aggregates by reconfiguration of energy metabolism [22]. The results from the current study demonstrate that aggregation enhances cell survival by *PI3K* activation through reconfiguration of energy metabolism and redox cycle.

In the current study, IA delivery with a microneedle provides a direct and safe route to the brain without passing through systemic organs, providing better survival and engraftment [56,57]. Longitudinal analysis using high-field MRI coupled with behavior analysis provides direct evidence of the impact of Agg-D hMSCs on lesion and functional recovery *in vivo* following MCAO. hMSCs labeled with MPIO were visualized with a T_2^*-weighted sequence, and MRI rendering of initial biodistribution of IA-delivered hMSCs immediately after injection showed homing to ipsilateral stroke hemisphere (Figure 6). Using the increased sensitivity of a 21.1-T ultra-high-field magnet, volume and signal-based lesion recovery with ^{1}H and ^{23}Na MRI was monitored longitudinally on the same animals. 2D T_2^*W GRE images revealed reduced clearance of Agg-D hMSCs compared with 2D hMSCs, although the difference was not statistically significant. ^{1}H ADC measurements did show a significant difference between Agg-D hMSC and MCAO-PBS groups at day 7 for the ipsilateral side of the brain, confirming the enhanced recovery of MCAO. However, with the same cohort of animals, ^{23}Na MRI displayed a significant and immediate improvement in the ischemic lesion volume (Figure 6) for the application of Agg-D hMSCs compared with 2D hMSCs. Sodium distribution and homeostasis are major players in the cascade following ischemic events and therefore are potentially crucial biomarkers of not only stroke

evolution but also therapeutic efficacy. Conventionally, the necrotic core and salvageable penumbral tissue resulting from ischemia are evaluated with ^{1}H diffusion and perfusion sequences, respectively [58,59]. Although providing information about cell size changes and blood flow, these indirect measures of water distributions lend inaccuracy to the measurement of evolving stroke lesion size and do not assess cellular function [60]. As a result, most ^{1}H MRI evaluations of MSCs in the treatment of stroke have not yielded significant findings or differences between pre-conditioning regiments based solely on MRI measures [24,61], in agreement with the current study. With sodium, differences in stroke evolution [62,63] and treatment efficacy [64] can be made directly and significantly evaluated. Wetterling *et al.* discovered a high sodium signal in the nonacute stroke phase that was not evident through ^{1}H MRI, which was attributed to necrotic tissue unrelated to the cell swelling on which ^{1}H MRI measurements rely [65]. This study hinted that sodium and its role in stroke pathology is a potentially better marker for stroke lesion recovery and can detect pathological changes before ^{1}H MRI. The current study takes advantage of ultra-high magnetic field to increase the sensitivity of sodium MRI, which has been demonstrated as a 3.0-fold gain between 9.4 and 21.1 T [26]. With this sensitivity, differences between 2D cultured and aggregated hMSC expansion were demonstrated with stroke recovery. In addition, the therapeutic response of the hMSCs as shown in this study corresponds to their ability to restore the ionic homeostasis by release of cytokines and trophic factors that consequently lead to reduced apoptosis [66].

For the cells to be visualized with MRI, a contrast agent and dose were chosen based on our previous studies, which evaluated the optimal balance between detectability and cellular properties [33,67]. Although some degree of particle release is expected when injecting MPIO-labeled hMSCs because of the activity of endogenous macrophages, GRE images remain a reliable measurement of relative persistence of the transplanted hMSC at the lesion site. Even though *in vivo* data demonstrate a significant reduction of labeled hMSC from the initial biodistribution at 24 h for both hMSC treatments, the high-resolution, 3D GRE image demonstrates the retention of MPIO contrast, reflecting the persistence of implanted hMSC out to 7 days. The relatively fast hMSCs clearance (Figure 6C) could have several explanations. It has been found that transplanted neuronal stem cells at 24 h post-ischemic events are more likely to be phagocytized in the ischemic brain [68]. The timing of the injection after ischemia affects the distribution of the cells and their consequent therapeutic response. Ishizaka *et al.* showed that IA-transplanted hMSCs 1 day after stroke were distributed in the infarct and peri-infarct region as evaluated with histological samples [69]. Three days later, an approximate 40% decrease of cells was observed. These previous results agree with the data presented in this study: an early transplantation still promotes stroke lesion recovery (with faster recovery for Agg-D hMSC group) but with relatively quick cell clearance.

The *in vitro* analysis and *in vivo* MR studies conducted in this work support the enhanced benefit of 3D aggregation over the conventional 2D monolayer culture of hMSCs under normoxic conditions. As our results of 2D hMSC demonstrated no significant improvement and previous studies of 2D cultured MSCs displayed no improvement in rat motor function, neurological or somatosensory recovery after MCAO [18, 24], the behavioral tests of this study focused on comparing functional improvements offered by Agg-D hMSCs against sham and untreated MCAO rats. Anxiety-related tests such as open-field and elevated plus maze also demonstrated the recovery of neurological functions in the Agg-D hMSC group. OFT has been widely used to assess locomotion and motor function post-ischemia [70]. The current results showed that MCAO animals with PBS or with Agg-D hMSC transplantation have decreased locomotion up to 16 days compared with sham animals, but the Agg-D hMSC group starts to show gradual recovery and better locomotion activity with more exploration at week 3, but no significant improvement of time spent in different zones, as shown in Figure 7. Although the enhanced locomotion and exploration of animals with Agg-D hMSC transplantation may indicate the recovery of neurological functions, studies also suggested that animals assessed with OFT often exhibit a hyperactivity developing around 3 weeks after surgery, which could influence the characterization of behavior for MCAO animals [71,72]. EPM can be used to evaluate anxiety-related behavior or memory loss due to cerebral trauma [73]. In this study, stroke animals with Agg-D hMSC transplantation start to show significantly improved EPM locomotor activity at week 3. With more entries in open arms and less time spent in the closed arm at week 4, the Agg-D hMSC group expressed less anxiety, which is not observed in OFT (Figure 7). These results correspond to the spontaneous forelimb use assessed via the cylinder test, which is used to investigate spatial and motor functions of stroke models [74,75]. Although sham control animals displayed slightly imbalanced use of forelimbs, the asymmetry score was close to zero [75]. The Agg-D hMSC group showed a decrease of asymmetry score from week 1, but significance

appears at week 3 compared with the MCAO-PBS group, which shows no reduction of the balance scores even after 4 weeks. As the behavioral results demonstrated, reduced motor deficits are attributed to the administration of Agg-D hMSCs immediately after MCAO, with early neuroprotection and enhanced survival of transplanted hMSCs [69,76].

The current study has some limitations. First, Agg-D or 2D hMSCs were injected immediately following the establishment of transient ischemia after a 1-h occlusion. In a clinical scenario, it is unlikely that any cell therapy would be introduced this rapidly during the acute phase of ischemia. As an initial foray into evaluating the efficacy of Agg-D hMSCs, this time point of intervention was chosen to develop a baseline of therapeutic response before evaluating more extended windows of treatment or multiple injections. Additionally, immediate injection of cells after the removal of the occluding filament facilitated this study in that multiple neck incisions were not required, minimizing excessive scar tissue formation, pain and distress. Second, the number of animals available for the final analysis of behavioral characteristics are low due to losses during the 4 weeks of experiments. However, the power of the measurement was maintained even with reduced sample size due to increases in the maximum differences between group means and lower standard deviations. Future studies will use the therapeutic response demonstrated here for Agg-D hMSCs as a foundation for evaluating extend windows of application during the subacute and chronic phases of cerebral ischemic to translate the apparent benefits of this approach to clinical realization.

Short-term aggregation enhances hMSC therapeutic properties in stroke treatment by restoring energy homeostasis and innate cellular properties. The study underscores the utility of high-field MRI to resolve differences between cell therapy efficacies in combination with behavioral analyses. Aggregation preconditioning following culture expansion is an implementable strategy in the translation of hMSC therapy for stroke treatment.

Acknowledgements

This work is supported by the National Institutes of Health (NIH; R01 NS102395) and National Science Foundation (NSF; CBET 1743426). The content is solely the responsibility of the authors and does not necessarily represent the official views of the NIH and NSF. A portion of this work was performed at the National High Magnetic Field Laboratory, which is supported by the NSF (DMR-1644779 and DMR-1157490) and the state of Florida.

Disclosure of interests: The authors have no commercial, proprietary or financial interest in the products or companies described in this article.

References

[1] Writing Group, M, Mozaffarian D, Benjamin EJ, Go AS, Arnett DK, Blaha MJ, et al. Heart Disease and Stroke Statistics-2016 Update: A Report From the American Heart Association. Circulation 2016;133:e38.

[2] Mozaffarian D, Benjamin EJ, Go AS, Arnett DK, Blaha MJ, Cushman M, et al. Heart disease and stroke statistics—2015 update: a report from the American Heart Association. Circulation 2015;131:e29.

[3] Stonesifer C, Corey S, Ghanekar S, Diamandis Z, Acosta SA, Borlongan CV. Stem cell therapy for abrogating stroke-induced neuroinflammation and relevant secondary cell death mechanisms. Progress in neurobiology 2017;158:94.

[4] Daadi MM, Maag AL, Steinberg GK. Adherent self-renewable human embryonic stem cell-derived neural stem cell line: functional engraftment in experimental stroke model. PloS one 2008;3:e1644.

[5] Yang D, Zhang ZJ, Oldenburg M, Ayala M, Zhang SC. Human embryonic stem cell-derived dopaminergic neurons reverse functional deficit in parkinsonian rats. Stem cells 2008;26:55.

[6] Nakagomi N, Nakagomi T, Kubo S, Nakano-Doi A, Saino O, Takata M, et al. Endothelial cells support survival, proliferation, and neuronal differentiation of transplanted adult ischemia-induced neural stem/progenitor cells after cerebral infarction. Stem cells 2009;27:2185.

[7] Kim DY, Park SH, Lee SU, Choi DH, Park HW, Paek SH, et al. Effect of human embryonic stem cell-derived neuronal precursor cell transplantation into the cerebral infarct model of rat with exercise. Neuroscience research 2007;58:164.

[8] Capowski EE, Schneider BL, Ebert AD, Seehus CR, Szulc J, Zufferey R, et al. Lentiviral vector-mediated genetic modification of human neural progenitor cells for ex vivo gene therapy. Journal of neuroscience methods 2007;163:338.

[9] Copland IB, Galipeau J. Death and inflammation following somatic cell transplantation. Seminars in immunopathology 2011;33:535.

[10] Bara JJ, Richards RG, Alini M, Stoddart MJ. Concise review: bone marrow-derived mesenchymal stem cells change phenotype following in vitro culture: implications for basic research and the clinic. Stem cells 2014;32:1713.

[11] Sart S, Ma T, Li Y. Preconditioning stem cells for in vivo delivery. BioResearch open access 2014;3:137.

[12] Sun J, Wei ZZ, Gu X, Zhang JY, Zhang Y, Li J, et al. Intranasal delivery of hypoxia-preconditioned bone marrow-derived mesenchymal stem cells enhanced regenerative effects after intracerebral hemorrhagic stroke in mice. Experimental neurology 2015;272:78.

[13] Pasha Z, Wang Y, Sheikh R, Zhang D, Zhao T, Ashraf M. Preconditioning enhances cell survival and differentiation of stem cells during transplantation in infarcted myocardium. Cardiovascular research 2008;77:134.

[14] Zemani F, Silvestre JS, Fauvel-Lafeve F, Bruel A, Vilar J, Bieche I, et al. Ex vivo priming of endothelial progenitor cells with SDF-1 before transplantation could increase their proangiogenic potential. Arteriosclerosis, thrombosis, and vascular biology 2008;28:644.

[15] Cui X, Wang H, Guo H, Wang C, Ao H, Liu X, et al. Transplantation of mesenchymal stem cells preconditioned with diazoxide, a mitochondrial ATP-sensitive potassium channel opener, promotes repair of myocardial infarction in

rats. The Tohoku journal of experimental medicine 2010;220:139.
[16] Afzal MR, Haider H, Idris NM, Jiang S, Ahmed RP, Ashraf M. Preconditioning promotes survival and angiomyogenic potential of mesenchymal stem cells in the infarcted heart via NF-kappaB signaling. Antioxidants & redox signaling 2010;12:693.
[17] Yao Y, Zhang F, Wang L, Zhang G, Wang Z, Chen J, et al. Lipopolysaccharide preconditioning enhances the efficacy of mesenchymal stem cells transplantation in a rat model of acute myocardial infarction. Journal of biomedical science 2009;16:74.
[18] Wei L, Fraser JL, Lu ZY, Hu X, Yu SP. Transplantation of hypoxia preconditioned bone marrow mesenchymal stem cells enhances angiogenesis and neurogenesis after cerebral ischemia in rats. Neurobiol Dis 2012;46:635.
[19] Herberts CA, Kwa MS, Hermsen HP. Risk factors in the development of stem cell therapy. Journal of translational medicine 2011;9:29.
[20] Sart S, Tsai AC, Li Y, Ma T. Three-dimensional aggregates of mesenchymal stem cells: cellular mechanisms, biological properties, and applications. Tissue engineering Part B, Reviews 2014;20:365.
[21] Lee RH, Pulin AA, Seo MJ, Kota DJ, Ylostalo J, Larson BL, et al. Intravenous hMSCs improve myocardial infarction in mice because cells embolized in lung are activated to secrete the anti-inflammatory protein TSG-6. Cell stem cell 2009;5:54.
[22] Liu Y, Munoz N, Tsai AC, Logan TM, Ma T. Metabolic Reconfiguration Supports Reacquisition of Primitive Phenotype in Human Mesenchymal Stem Cell Aggregates. Stem cells 2017;35:398.
[23] Kim JH, Park IS, Park Y, Jung Y, Kim SH, Kim SH. Therapeutic angiogenesis of three-dimensionally cultured adipose-derived stem cells in rat infarcted hearts. Cytotherapy 2013;15:542.
[24] Guo L, Ge J, Zhou Y, Wang S, Zhao RC, Wu Y. Three-dimensional spheroid-cultured mesenchymal stem cells devoid of embolism attenuate brain stroke injury after intra-arterial injection. Stem cells and development 2014;23:978.
[25] Nagel AM, Umathum R, Rosler MB, Ladd ME, Litvak I, Gor'kov PL, et al. (39) K and (23) Na relaxation times and MRI of rat head at 21.1 T. NMR in biomedicine 2016;29:759.
[26] Schepkin VD, Brey WW, Gor'kov PL, Grant SC. Initial in vivo rodent sodium and proton MR imaging at 21.1 T. Magnetic resonance imaging 2010;28:400.
[27] Wetterling F, Gallagher L, Macrae IM, Junge S, Fagan AJ. Regional and temporal variations in tissue sodium concentration during the acute stroke phase. Magnetic resonance in medicine 2012;67:740.
[28] Astrup J, Siesjo BK, Symon L. Thresholds in cerebral ischemia—the ischemic penumbra. Stroke 1981;12:723.
[29] Liu Y, Munoz N, Bunnell BA, Logan TM, Ma T. Density-dependent metabolic heterogeneity in human mesenchymal stem cells. Stem cells 2015;33:3368.
[30] Tsai AC, Liu Y, Yuan X, Ma T. Compaction, fusion, and functional activation of three-dimensional human mesenchymal stem cell aggregate. Tissue engineering Part A 2015;21:1705.
[31] Uluc K, Miranpuri A, Kujoth GC, Akture E, Baskaya MK. Focal cerebral ischemia model by endovascular suture occlusion of the middle cerebral artery in the rat. Journal of visualized experiments: JoVE 2011.
[32] Longa EZ, Weinstein PR, Carlson S, Cummins R. Reversible Middle Cerebral-Artery Occlusion without Craniectomy in Rats. Stroke 1989;20:84.
[33] Rosenberg JT, Sellgren KL, Sachi-Kocher A, Calixto Bejarano F, Baird MA, Davidson MW, et al. Magnetic resonance contrast and biological effects of intracellular superparamagnetic iron oxides on human mesenchymal stem cells with long-term culture and hypoxic exposure. Cytotherapy 2013;15:307.
[34] Rosenberg J, Yuan X, Grant S, Ma T. Tracking mesenchymal stem cells using magnetic resonance imaging. Brain Circulation 2016;2:108.
[35] Fu R, Brey WW, Shetty K, Gor'kov P, Saha S, Long JR, et al. Ultra-wide bore 900 MHz high-resolution NMR at the National High Magnetic Field Laboratory. Journal of magnetic resonance 2005;177:1.
[36] Tsai AC, Liu Y, Yuan X, Chella R, Ma T. Aggregation kinetics of human mesenchymal stem cells under wave motion. Biotechnology journal 2017;12.
[37] Yuan X, Tsai AC, Farrance I, Rowley J, Ma T. Aggregation of Culture Expanded Human Mesenchymal Stem Cells in Microcarrier-based Bioreactor. Biochem Eng J 2018;131:39.
[38] Mounayar M, Kefaloyianni E, Smith B, Solhjou Z, Maarouf OH, Azzi J, et al. PI3kalpha and STAT1 Interplay Regulates Human Mesenchymal Stem Cell Immune Polarization. Stem cells 2015;33:1892.
[39] Sohni A, Verfaillie CM. Mesenchymal stem cells migration homing and tracking. Stem cells international 2013;2013:130763.
[40] Karp JM, Leng Teo GS. Mesenchymal stem cell homing: the devil is in the details. Cell stem cell 2009;4:206.
[41] Chen J, Li Y, Wang L, Lu M, Zhang X, Chopp M. Therapeutic benefit of intracerebral transplantation of bone marrow stromal cells after cerebral ischemia in rats. Journal of the neurological sciences 2001;189:49.
[42] Bonab MM, Alimoghaddam K, Talebian F, Ghaffari SH, Ghavamzadeh A, Nikbin B. Aging of mesenchymal stem cell in vitro. BMC cell biology 2006;7:14.
[43] Toma C, Wagner WR, Bowry S, Schwartz A, Villanueva F. Fate of culture-expanded mesenchymal stem cells in the microvasculature: in vivo observations of cell kinetics. Circulation research 2009;104:398.
[44] Galipeau J. The mesenchymal stromal cells dilemma—does a negative phase III trial of random donor mesenchymal stromal cells in steroid-resistant graft-versus-host disease represent a death knell or a bump in the road? Cytotherapy 2013;15:2.
[45] Janowski M, Lyczek A, Engels C, Xu J, Lukomska B, Bulte JW, et al. Cell size and velocity of injection are major determinants of the safety of intracarotid stem cell transplantation. Journal of cerebral blood flow and metabolism 2013;33:921.
[46] Ge J, Guo L, Wang S, Zhang Y, Cai T, Zhao RC, et al. The size of mesenchymal stem cells is a significant cause of vascular obstructions and stroke. Stem cell reviews 2014;10:295.
[47] Bijonowski, MBM, Daraiseh, DSI, Yuan, MX, Ma, D.T. Size-dependent cortical compaction induces metabolic adaptation in mesenchymal stem cell aggregates. Tissue Engineering Part A 0, null.
[48] Pennock R, Bray E, Pryor P, James S, McKeegan P, Sturmey R, et al. Human cell dedifferentiation in mesenchymal condensates through controlled autophagy. Scientific reports 2015;5:13113.
[49] Mo M, Zhou Y, Li S, Wu Y. Three-dimensional culture reduces cell size by increasing vesicle excretion. Stem cells 2018;36:286.
[50] Liu Y, Tsai A-C, Yuan X, Li Y, Ma T. Chapter 18—hypoxia regulation of stem cell: mechanisms, biological properties, and applications. In: Vishwakarma A, Karp JM, eds. Biology and Engineering of Stem Cell Niches, Boston: Academic Press; 2017. p. 273.

[51] Chen J, Crawford R, Chen C, Xiao Y. The key regulatory roles of the PI3K/Akt signaling pathway in the functionalities of mesenchymal stem cells and applications in tissue regeneration. Tissue engineering Part B, Reviews 2013;19:516.
[52] Stubbs SL, Hsiao ST, Peshavariya HM, Lim SY, Dusting GJ, Dilley RJ. Hypoxic preconditioning enhances survival of human adipose-derived stem cells and conditions endothelial cells in vitro. Stem cells and development 2012;21:1887.
[53] Wang ZJ, Zhang FM, Wang LS, Yao YW, Zhao Q, Gao X. Lipopolysaccharides can protect mesenchymal stem cells (MSCs) from oxidative stress-induced apoptosis and enhance proliferation of MSCs via Toll-like receptor(TLR)-4 and PI3K/Akt. Cell Biol Int 2009;33:665.
[54] Pelicano H, Xu RH, Du M, Feng L, Sasaki R, Carew JS, et al. Mitochondrial respiration defects in cancer cells cause activation of Akt survival pathway through a redox-mediated mechanism. The Journal of cell biology 2006;175:913.
[55] Liu Y, Yuan X, Muñoz N, Logan TM, Ma T. Commitment to Aerobic Glycolysis Sustains Immunosuppression of Human Mesenchymal Stem Cells. STEM CELLS Translational Medicine 2019;8:93.
[56] Chua JY, Pendharkar AV, Wang N, Choi R, Andres RH, Gaeta X, et al. Intra-arterial injection of neural stem cells using a microneedle technique does not cause microembolic strokes. Journal of cerebral blood flow and metabolism: official journal of the International Society of Cerebral Blood Flow and Metabolism 2011;31:1263.
[57] Lundberg J, Sodersten E, Sundstrom E, Le Blanc K, Andersson T, Hermanson O, et al. Targeted intra-arterial transplantation of stem cells to the injured CNS is more effective than intravenous administration: engraftment is dependent on cell type and adhesion molecule expression. Cell transplantation 2012;21:333.
[58] Sobesky J, Zaro Weber O, Lehnhardt FG, Hesselmann V, Neveling M, Jacobs A, et al. Does the mismatch match the penumbra? Magnetic resonance imaging and positron emission tomography in early ischemic stroke. Stroke 2005;36:980.
[59] Heiss WD, Sobesky J. Comparison of PET and DW/PW-MRI in acute ischemic stroke. The Keio journal of medicine 2008;57:125.
[60] Lin SP, Song SK, Miller JP, Ackerman JJ, Neil JJ. Direct, longitudinal comparison of (1)H and (23)Na MRI after transient focal cerebral ischemia. Stroke 2001;32:925.
[61] Li WY, Choi YJ, Lee PH, Huh K, Kang YM, Kim HS, et al. Mesenchymal stem cells for ischemic stroke: changes in effects after ex vivo culturing. Cell transplantation 2008;17:1045.
[62] Hussain MS, Stobbe RW, Bhagat YA, Emery D, Butcher KS, Manawadu D, et al. Sodium imaging intensity increases with time after human ischemic stroke. Annals of neurology 2009;66:55.
[63] Jones SC, Kharlamov A, Yanovski B, Kim DK, Easley KA, Yushmanov VE, et al. Stroke onset time using sodium MRI in rat focal cerebral ischemia. Stroke 2006;37:883.
[64] LaVerde GC, Jungreis CA, Nemoto E, Boada FE. Sodium time course using 23Na MRI in reversible focal brain ischemia in the monkey. Journal of magnetic resonance imaging: JMRI 2009;30:219.
[65] Wetterling F, Ansar S, Handwerker E. Sodium-23 magnetic resonance imaging during and after transient cerebral ischemia: multinuclear stroke protocols for double-tuned (23)Na/(1)H resonator systems. Physics in medicine and biology 2012;57:6929.
[66] Chen J, Li Y, Katakowski M, Chen X, Wang L, Lu D, et al. Intravenous bone marrow stromal cell therapy reduces apoptosis and promotes endogenous cell proliferation after stroke in female rat. Journal of neuroscience research 2003;73:778.
[67] Rosenberg JT, Kogot JM, Lovingood DD, Strouse GF, Grant SC. Intracellular bimodal nanoparticles based on quantum dots for high-field MRI at 21.1 T. Magnetic resonance in medicine 2010;64:871.
[68] Zhang Z, Chopp M. Neural Stem Cells and Ischemic Brain. Journal of stroke 2016;18:267.
[69] Ishizaka S, Horie N, Satoh K, Fukuda Y, Nishida N, Nagata I. Intra-arterial cell transplantation provides timing-dependent cell distribution and functional recovery after stroke. Stroke 2013;44:720.
[70] Belzung C, Griebel G. Measuring normal and pathological anxiety-like behaviour in mice: a review. Behavioural brain research 2001;125:141.
[71] Manwani B, Liu F, Xu Y, Persky R, Li J, McCullough LD. Functional recovery in aging mice after experimental stroke. Brain, behavior, and immunity 2011;25:1689.
[72] Balkaya M, Krober JM, Rex A, Endres M. Assessing post-stroke behavior in mouse models of focal ischemia. Journal of cerebral blood flow and metabolism 2013;33:330.
[73] Rehni AK, Singh N, Jaggi AS, Singh M. Amniotic fluid derived stem cells ameliorate focal cerebral ischaemia-reperfusion injury induced behavioural deficits in mice. Behavioural brain research 2007;183:95.
[74] Markgraf CG, Green EJ, Hurwitz BE, Morikawa E, Dietrich WD, McCabe PM, et al. Sensorimotor and cognitive consequences of middle cerebral artery occlusion in rats. Brain research 1992;575:238.
[75] Schallert T, Fleming SM, Leasure JL, Tillerson JL, Bland ST. CNS plasticity and assessment of forelimb sensorimotor outcome in unilateral rat models of stroke, cortical ablation, parkinsonism and spinal cord injury. Neuropharmacology 2000;39:777.
[76] van Velthoven CT, Sheldon RA, Kavelaars A, Derugin N, Vexler ZS, Willemen HL, et al. Mesenchymal stem cell transplantation attenuates brain injury after neonatal stroke. Stroke 2013;44:1426.